Journal of Nuclear Medicine, published on November 9, 2023 as doi:10.2967/jnumed.123.266388

^{212}Pb-Pretargeted Theranostics for Pancreatic Cancer

David Bauer[1], Lukas M. Carter[2], Mohamed I. Atmane[3], Roberto De Gregorio[1], Alexa Michel[1], Spencer Kaminsky[1], Sebastien Monette[3], Mengshi Li[4], Michael K. Schultz[4], and Jason S. Lewis[1,5]

[1]Department of Radiology and Molecular Pharmacology Program, Memorial Sloan Kettering Cancer Center, New York, New York; [2]Department of Medical Physics, Memorial Sloan Kettering Cancer Center, New York, New York; [3]Laboratory of Comparative Pathology, Memorial Sloan Kettering Cancer Center, Weill Cornell Medicine, and Rockefeller University, New York, New York; [4]Perspective Therapeutics, Inc., Coralville, Iowa; and [5]Department of Radiology and Pharmacology Program, Weill Cornell Medical College, New York, New York

Although pancreatic ductal adenocarcinoma (PDAC) is associated with limited treatment options and poor patient outcomes, targeted α-particle therapy (TAT) represents a promising development in the field. TAT shows potential in treating metastatic cancers, including those that have become resistant to conventional treatments. Among the most auspicious radionuclides stands the in vivo α-generator ^{212}Pb. Combined with the imaging-compatible radionuclide ^{203}Pb, this theranostic match is a promising modality rapidly translating into the clinic. **Methods:** Using the pretargeting approach between a radiolabeled 1,2,4,5-tetrazine (Tz) tracer and a *trans*-cyclooctene (TCO) modified antibody, imaging and therapy with radiolead were performed on a PDAC tumor xenograft mouse model. For therapy, 3 cohorts received a single administration of 1.1, 2.2, or 3.7 MBq of the pretargeting agent, [^{212}Pb]Pb-DO3A-PEG$_7$-Tz, whereby administered activity levels were guided by dosimetric analysis. **Results:** The treated mice were holistically evaluated; minimal-to-mild renal tubular necrosis was observed. At the same time, median survival doubled for the highest-dose cohort (10.7 wk) compared with the control cohort (5.1 wk). **Conclusion:** This foundational study demonstrated the feasibility and safety of pretargeted TAT with ^{212}Pb in PDAC while considering dose limitations and potential adverse effects.

Key Words: targeted α-therapy; pretargeting; lead-212; progeny release; lead-203

J Nucl Med 2024; 00:1–8
DOI: 10.2967/jnumed.123.266388

Recent advances in oncology have led to marked improvements in the standard of care for cancer patients. Nevertheless, metastatic relapse remains the principal cause of cancer mortality (*1*).

Targeted α-particle therapy (TAT) is thought to provide optimal properties for treating disseminated micrometastatic diseases and exhibits significant potential, especially for tackling rapidly progressing cancers (*2–4*). TAT aims to selectively deliver α radiation to cancer cells while minimizing treatment-related toxicities. The direct cell-killing effect of α-particles is related to the induction of double-stranded DNA ruptures caused by the impact of the massive particles combined with their high linear energy transfer (50–230 keV/μm). Because of their relatively short effective range (<100 μm), α-emitters minimally cross-irradiate surrounding healthy tissue (*5*).

One increasingly popular radionuclide is the in vivo α-particle generator ^{212}Pb, which emits 1 (net) α-particle and 2 β^--particles within its decay chain (Fig. 1; Supplemental Fig. 1; supplemental materials are available at http://jnm.snmjournals.org). An isotopic theranostic match can be found in ^{203}Pb, which has a half-life of 2.1 d and is suitable for SPECT imaging. Because of the pair's suitable chemical and physical properties, ^{203}Pb and ^{212}Pb are ideal for clinical translation (*6*). However, with a relatively short physical half-life (10.6 h), ^{212}Pb-bearing radiopharmaceuticals require fast pharmacokinetics. Thus, pretargeted radionuclide therapy (PRT) is an especially promising strategy for using ^{212}Pb (*7*).

Our laboratories previously reported the inverse electron-demand Diels-Alder ligation's potential for PRT (*8–11*). In this work, we investigated the pretargeting strategy between the trans-cyclooctene (TCO)–conjugated monoclonal antibody (mAb) 5B1 and ^{212}Pb-radiolabeled Tz conjugates. 5B1 targets the carbohydrate cell surface antigen 19-9, which is overexpressed in pancreatic ductal adenocarcinoma (PDAC)—a uniformly lethal cancer form with limited treatment options (*12*). The pretargeting approach decouples the relatively short physical half-life of the radionuclide from the long biologic half-life of antibodies, promising both high specific binding to the tumor marker and fast clearance of the radiotracer. In a preclinical model, we aimed to prove that this strategy rapidly and safely delivers ^{212}Pb to the tumor. A further advantage of pretargeting is that multiple Tz radiotracers can be subsequently administered with almost identical tumor uptake, as previously reported (*9*). This allows for delivering a diagnostic Tz tracer first and calculating dosimetry estimates, followed by administering the therapeutic one without reinjecting the mAb (Fig. 1). This approach will enable clinicians to better anticipate the outcome of therapy preceded by predictive imaging.

MATERIALS AND METHODS

Information about laboratory equipment, biology, dosimetry, and additional studies can be found in the supplemental materials, as well as the synthesis of the Tz precursors modified with a polyethylene glycol 7 (PEG_7) linker and attached to one of the 4 chelators: TCMC (2-[4,7,10-tris(2-amino-2-oxoethyl)-1,4,7,10-tetrazacyclododec-1-yl]acetamide), PSC (2-[4,10-bis(carboxymethyl)-1,4,7,10-tetrazacyclododec-1-yl]-acetamide), DO3A (1,4,7,10-tetraazacyclododecane-1,4,7-triacetic acid), or DOTA (2,2′,2′′,2′′′-(1,4,7,10-tetraazacyclododecane-1,4,7,10-tetrayl)-tetraacetic acid).

All animal procedures were approved by the Institutional Animal Care and Use Committee.

Received Jul. 24, 2023; revision accepted Sep. 28, 2023.
For correspondence or reprints, contact Jason S. Lewis (lewisj2@mskcc.org).
Published online Nov. 9, 2023.

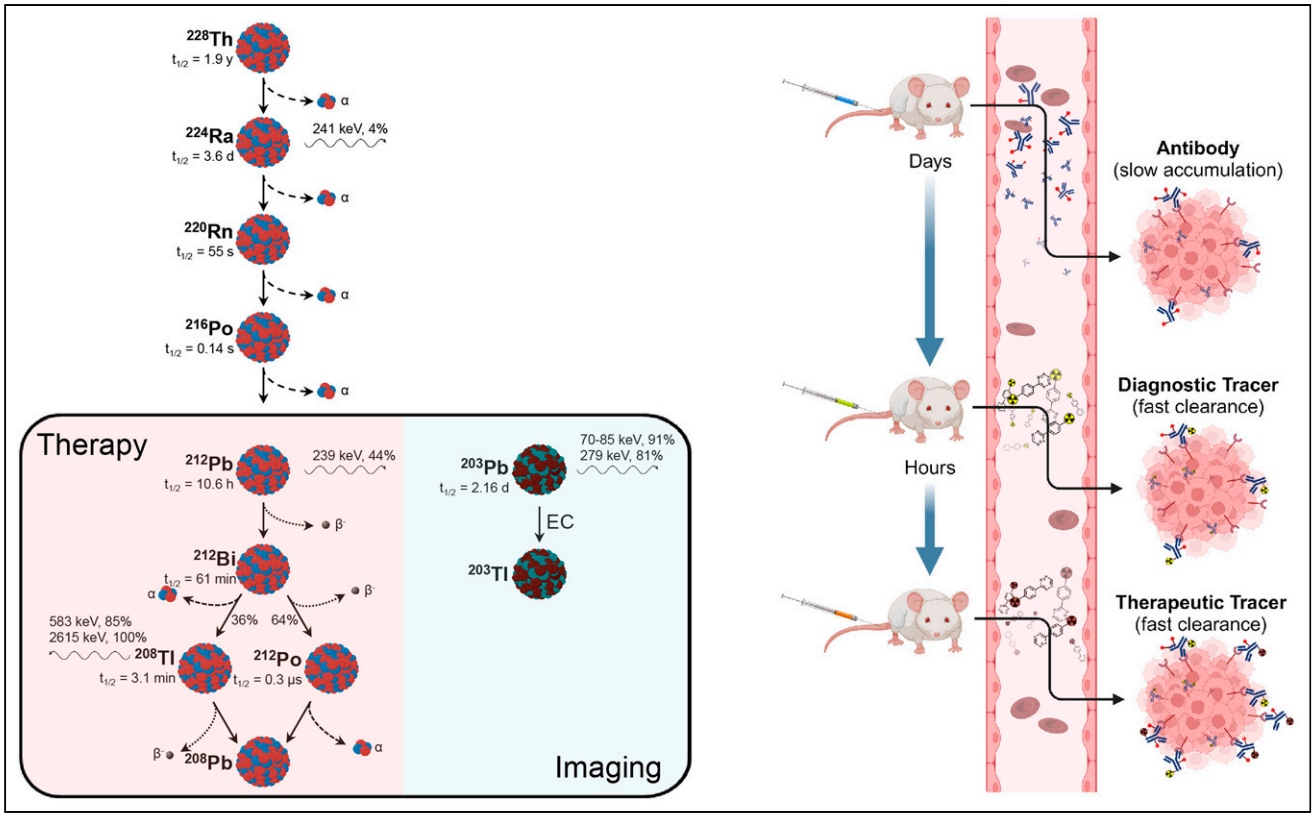

FIGURE 1. Pretargeting with theranostic pair ^{203}Pb and ^{212}Pb. (Left) Decay scheme of in vivo α-generator ^{212}Pb and SPECT-compatible nuclide ^{203}Pb. (Right) Illustration of theranostic pretargeting approach, following concept of reference *9*. This figure was created with BioRender. EC = electron capture; $t_{1/2}$ = half-life.

General Information for In Vivo Studies

For pharmacokinetic assessments, the ^{203}Pb- or ^{64}Cu-labeled Tz was intravenously injected (tail vain) into 8 healthy female athymic nude mice, and the radiotracer distribution was determined in selected organs at 1 and 4 h after injection (n = 4 per time point). The mice were intravenously injected with the 5B1-TCO conjugate (100 μg in sterile filtered phosphate-buffered saline) for pretargeting. Three to 4 d later, the mice received the radiolabeled tracer (2 nmol in phosphate-buffered saline).

Imaging

The mice were anesthetized using 2% isoflurane for imaging. SPECT/CT images with ^{203}Pb (11–37 MBq per mouse) were obtained on a Mediso nanoScan SPECT/CT device equipped with a high-resolution, low-energy, multipinhole collimator detecting the ^{203}Pb characteristic x-rays between 70 and 90 keV. All SPECT images were analyzed using VivoQuant (Invicro) reconstruction software (2020patch1hf2). PET/CT images with ^{64}Cu (~7.4 MBq per mouse) were obtained on an Inveon PET/CT (Siemens) rodent scanner. All PET/CT images were analyzed using the Inveon software suite. The counting rates in the reconstructed images were converted to the mean percentage injected dose per gram of tissue (%ID/g) by applying a system-specific calibration factor. Cerenkov luminescence imaging with ^{212}Pb (recording time, 5 min) was performed with an IVIS Spectrum (PerkinElmer).

For biodistribution studies, the mice were euthanized (CO_2 asphyxiation followed by cervical dislocation), and the tissues of interest were harvested for γ-counting or histologic analyses.

Therapy

A ^{212}Pb PRT dose escalation study was performed to evaluate therapeutic potential and identify potential adverse effects. Sixty mice were implanted with subcutaneous tumor xenografts 5 wk before the study commenced. The width and length of the tumors were determined using a caliper, and the tumor volume was calculated via Equation 1 as described in the literature (*13*).

$$\text{Tumor volume} = \frac{4}{3} \times \left(\frac{\text{length}}{2}\right)^2 \times \frac{\text{width}}{2}. \qquad \text{Eq. 1}$$

Mice with tumor volumes of 100–300 mm^3 were selected and randomized into 5 cohorts (n = 8 per cohort). Two cohorts served as controls and 3 received administered activities of 1.1, 2.2, and 3.7 MBq; the choice of these administered activities was guided by dosimetry estimates and accepted dosimetry thresholds for tumor response and toxicity (*14,15*). The mice received the 5B1-TCO conjugate 1 d after randomization and the ^{212}Pb-labeled Tz 3 d later. Wellness was monitored daily, and tumor volume and body weight were monitored biweekly until the endpoint. The endpoint was defined as a tumor volume of more than 2,000 mm^3, weight loss of more than 20% (compared with initial measurement), or a concerning health condition (e.g., necrotic or ulcerating tumor). After reaching their endpoints, the mice were euthanized, and selected tissues, including tumors, livers, and kidneys, were collected. Selected mice (n = 14 in total) from each cohort were submitted alive to a board-certified veterinary pathologist at the Memorial Sloan Kettering Cancer Center, Weill Cornell Medicine, and the Rockefeller University Laboratory of Comparative Pathology for a holistic evaluation. Blood samples (3 per cohort) were collected weekly via retroorbital blood draws and analyzed with a Hemavet 950 (Drew Scientific).

All data are represented as mean value ± standard error of the mean. The sample sizes were selected regarding statistical considerations,

ethical guidelines, and exigencies of funding. The significance analyses were performed using GraphPad Prism software 9.0, using unpaired 2-tailed *t*, multiple *t,* and log-rank tests.

RESULTS

Chemical Evaluation of Tz-Based Radiotracers

The pharmacokinetic properties of Tz-based radiopharmaceutical systems are essential factors for the success of PRT. Ideally, Tz-based radiopharmaceuticals exhibit short blood retention times and demonstrate low off-target uptake; usually, renal elimination is preferable. For this study, we investigated the previously developed precursor DOTA-PEG$_7$-Tz (*8*) and 3 additional precursors differing in the attached chelator (Fig. 2A). The 4 precursors are distinct in their theoretic charge (from +2 to −2, when lead-labeled), which might have a substantial influence on their pharmacokinetics (*16,17*). To visualize their relative ionic behavior under physiologic conditions, we performed paper electrophoresis with the ^{212}Pb-labeled radiotracers using phosphate-buffered saline at a pH of 7.4 (*18*), followed by phosphor imaging (Fig. 2B). Worthy of mentioning, the charges are not sharply defined but are a function of the pH and concentration of other coordinating anions and cations. Free Pb^{2+} hydrolyzes under physiologic conditions and predominately forms the $Pb(OH)^+$ species, thus explaining the minimal migration (*19*). The 4 radiotracers showed a clear charge tendency, with DO3A-PEG$_7$-Tz and PSC-PEG$_7$-Tz being close to their isoelectric point. It has been previously reported that a slight negative charge facilitates a beneficial pharmacokinetic behavior (*17,20*). These results suggest that DO3A-PEG$_7$-Tz might show superior performance in vivo, with a relatively short plasma retention time, fast renal clearance, and minimal hepatic clearance.

The radiotracers' lipophilicity was investigated by analytic high-performance liquid chromatography and confirmed by the 1-octanol/phosphate-buffered saline distribution coefficient at pH 7.4 (log $D_{7.4}$) (*21*). The data (Fig. 2C; Supplemental Table 1) affirm that all compounds are susceptible to high aqueous solubility and poor membrane permeability—desirable properties for a pretargeting tracer. The reason for the relatively similar behavior is that the lipophilicity is predominately regulated by the Tz-PEG$_7$ unit, which all compounds have in common.

All precursors (at a concentration of 10^{-6} M) demonstrated lead incorporation greater than 90% within 15 min at 37°C (Fig. 2D). Further experiments (Supplemental Fig. 2) revealed that a chelator concentration greater than 10^{-6} M and a chelator:metal ratio greater than 50:1 is required to approach quantitative labeling yield. The tracer stability of all ^{203}Pb-labeled tracers was investigated in human serum at 37°C via radio–instant thin-layer chromatography and revealed a release of less than 5% ^{203}Pb over 5 d, indicating that all lead chelates possess excellent stability.

Pharmacokinetics of Radiotracers

The ^{203}Pb-labeled and purified radiotracers (Supplemental Fig. 3) were administered to healthy mice, and their pharmacokinetic behavior was investigated (Fig. 3A). All tracers showed a predominantly renal clearance (>90 %ID/g, Supplemental Fig. 4). The TCMC-based tracer, with the highest positive relative charge in the paper electrophoresis, revealed slightly higher blood retention (0.71 ± 0.05 %ID/g at 1 h), possibly because of increased binding to the negatively charged albumin. Additionally, an

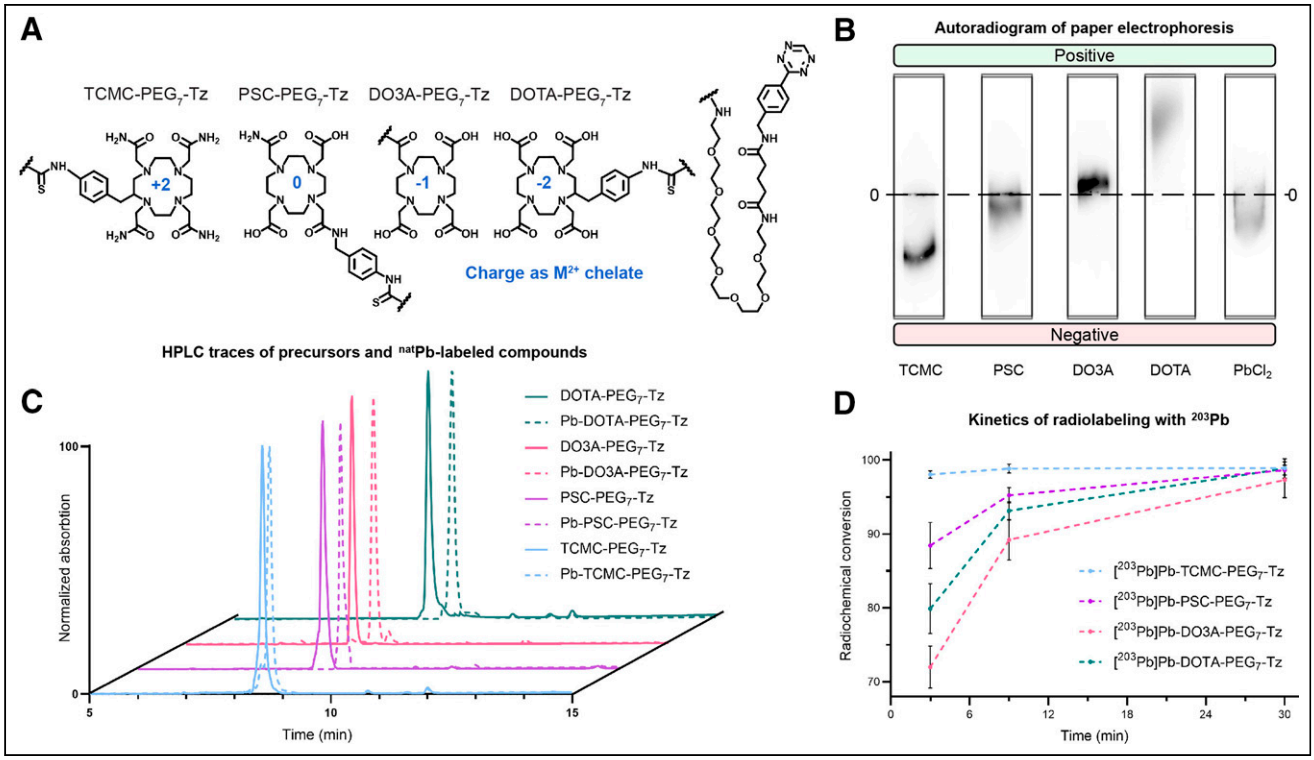

FIGURE 2. Chemical evaluation of Tz compounds. (A) Chemical structures of 4 Tz precursors. (B) Autoradiogram of paper electrophoresis performed with ^{212}Pb-labeled Tz precursors and [^{212}Pb]$PbCl_2$ at pH 7.4. (C) Normalized high-performance liquid chromatography diagrams of free and ^{nat}Pb-labeled Tz compounds (ultraviolet/visible light signal recorded at 254 nm). (D) Radiochemical conversion of Tz precursors (concentration of Tz = 10^{-6} mol/L, at 37°C) with ^{203}Pb measured via radio–instant thin-layer chromatography.

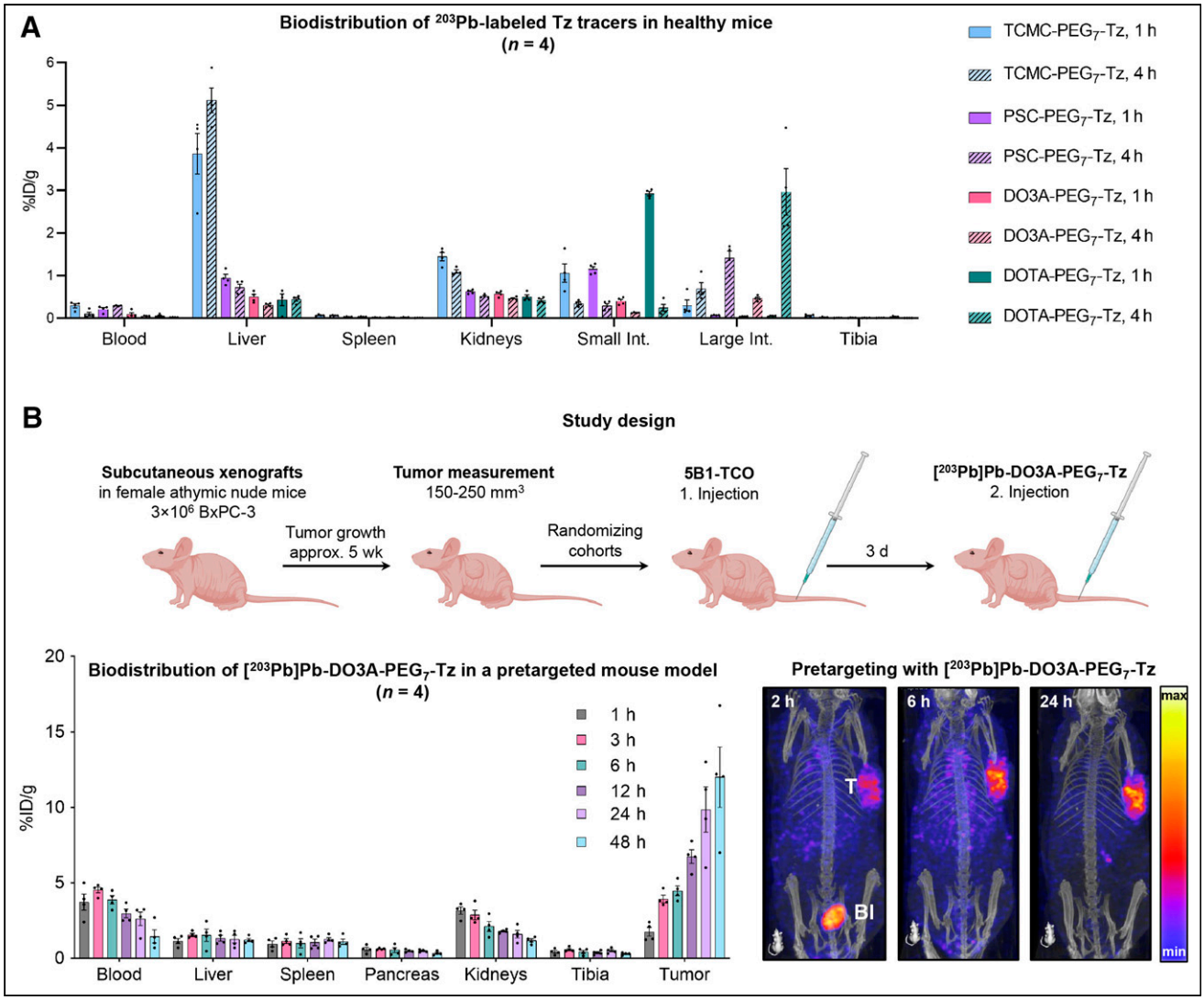

FIGURE 3. Pretargeting study with [^{203}Pb]Pb-DO3A-PEG$_7$-Tz. (A) Biodistribution data of 4 ^{203}Pb-labeled Tz tracers (2 nmol, 0.7 MBq) in healthy female nude mice. (B) Results of initial pretargeting study, with study design shown at top and, at bottom, biodistribution data of [^{203}Pb]Pb-DO3A-PEG$_7$-Tz (2 nmol, 0.7 MBq) in mice pretargeted with 5B1-TCO (100 μg, 0.7 nmol), accompanied by SPECT maximum-intensity projections (2 nmol, 18.5 MBq). Bl = bladder uptake; T = tumor uptake.

increased uptake in kidneys (3.0 ± 0.1 %ID/g at 4 h) and liver (3.5 ± 0.1 %ID/g at 4 h) was observed. The radiotracer with the highest relative negative charge, DOTA, showed partial hepatic clearance, as indicated by intestinal uptake (3.9 ± 0.3 %ID/g at 4 h). This clearance path is unfavorable because of the high radiosensitivity of the intestinal tract. The DO3A derivative showed the best pharmacokinetics, with fast clearance and low uptake in healthy tissue. Interestingly, this outcome could not have been predicted by relying solely on log$D_{7.4}$ values or in vitro stability tests. However, investigating the overall charge (visualized via paper electrophoresis) indicated which radiotracer could provide desirable pharmacokinetics; a slight negative charge (at pH 7.4) was confirmed to be beneficial for fast renal clearance.

Moving forward, the lead candidate, DO3A-PEG$_7$-Tz, radiolabeled with ^{203}Pb was investigated in a murine xenografted PDAC model pretargeted with 5B1-TCO (Fig. 3B). SPECT imaging and a multiple-time-point biodistribution study revealed a tumor uptake of 9.9 ± 1.4 %ID/g at 24 h after Tz injection. The tumor-to-blood ratio was 3.8 ± 1.0, and the tumor-to-muscle ratio at the same time was 27.2 ± 8.4. The increased blood retention (2.6 ± 0.4 %ID/g) can be attributed to still-circulating 5B1-TCO, which reacted with the Tz tracer and slowly accumulated at the tumor site. Within the 48-h interval, no release of ^{203}Pb was observed. These results reflect previously published pretargeting data (*9,22*).

^{212}Bi Release and Dosimetry Estimations

It is essential to underline that ^{212}Pb itself is not the α-emitter but its progeny. Since ^{212}Po has a short half-life of 0.3 μs, its redistribution can be neglected. However, the first daughter—^{212}Bi (half-life, 61 min)—has the potential to redistribute in the body. The conversion from ^{212}Pb to ^{212}Bi happens via low-energy β-decay, and the average recoil energy is approximately 0.52 eV. Hence, the ^{212}Bi release is unlikely to be driven by the recoil, assuming a bond energy of around 3 eV (*23*). However, the yield of conversion electrons from ^{212}Pb is relatively high (38%) and is followed by a cascade of Auger electrons resulting in highly

ionized states for the daughter nuclides (Bi^{4+} to Bi^{7+}), which are postulated to destroy the chelate (*24,25*). If ^{212}Bi is released from the tumor environment, it will localize predominantly in the kidneys (Supplemental Fig. 5) (*8,26*).

Using radiochemical separation methods (Supplemental Fig. 6), we determined via γ-spectroscopy (Supplemental Fig. 7) that on average 40% ± 5% of ^{212}Bi is eliminated from the chelators (Supplemental Table 2). This reflects values previously reported in the literature (*24,27–29*). However, when we were investigating the ^{212}Bi release in a cell assay using the BxPC-3 cell line (Supplemental Fig. 6B), instead of 40% ± 5% only 26% ± 5% unbound ^{212}Bi was detected in the cell medium. When we repeated this experiment but incubated the cells at 4°C, an increased fraction of 34% ± 5% ^{212}Bi was released. We hypothesize that biologic processes such as mitosis, membrane turnover, and endocytosis of the radiotracer facilitate the retention of unbound ^{212}Bi. The possibility of an active bismuth transport mechanism was ruled out by incubating the cells with [^{212}Bi]$BiCl_3$; no ^{212}Bi uptake was detected.

Finally, we investigated the release of ^{212}Bi in vivo using the pretargeting strategy with [^{212}Pb]Pb-DO3A-PEG_7-Tz in our PDAC xenograft mouse model. The mice were euthanized individually 24 h after injection of the radiotracer, and the tissues of interest were measured via γ-counting. We determined that merely 14.6% ± 0.7% of the intratumorally generated ^{212}Bi activity was redistributed. As expected, an additional relative uptake of 58.3% ± 6.4% ^{212}Bi activity (compared with ^{212}Pb) was measured in the kidneys (Fig. 4), reflecting the ^{212}Bi elimination from the tumor.

Summarizing, even though we determined an elimination of 40% ± 5% ^{212}Bi from the chelator, the release of intratumorally generated ^{212}Bi was reduced to 14.6% ± 0.7% in vivo, because of the retention of the progeny within the tumor environment.

Pretargeting dosimetry estimates for murine administration of [^{212}Pb]Pb-DO3A-PEG_7-Tz were determined according to the literature (Fig. 4) (*30–33*). When no daughter redistribution was assumed, the critical organs were the kidneys (6.9 Gy-equivalent/MBq of [^{212}Pb]Pb-DO3A-PEG_7-Tz administered), red marrow (9.5 Gy-equivalent/MBq), and urinary bladder (7.5 Gy-equivalent/MBq) (Supplemental Table 3). When using a conservative organ-level release estimate of 40% ^{212}Bi (highly overestimated as confirmed by the in vivo ^{212}Bi release study showing only 14.6% ± 0.7% release), which is followed by rapid redistribution and kidney accumulation, we calculated that the kidney dose coefficient could increase by nearly an order of magnitude (62 Gy-equivalent/MBq) (Supplemental Table 4). In contrast, dose coefficients for the tumor and other organs consequently decrease by 40%. In either case, myelotoxicity and renal toxicity are determining dose limitations.

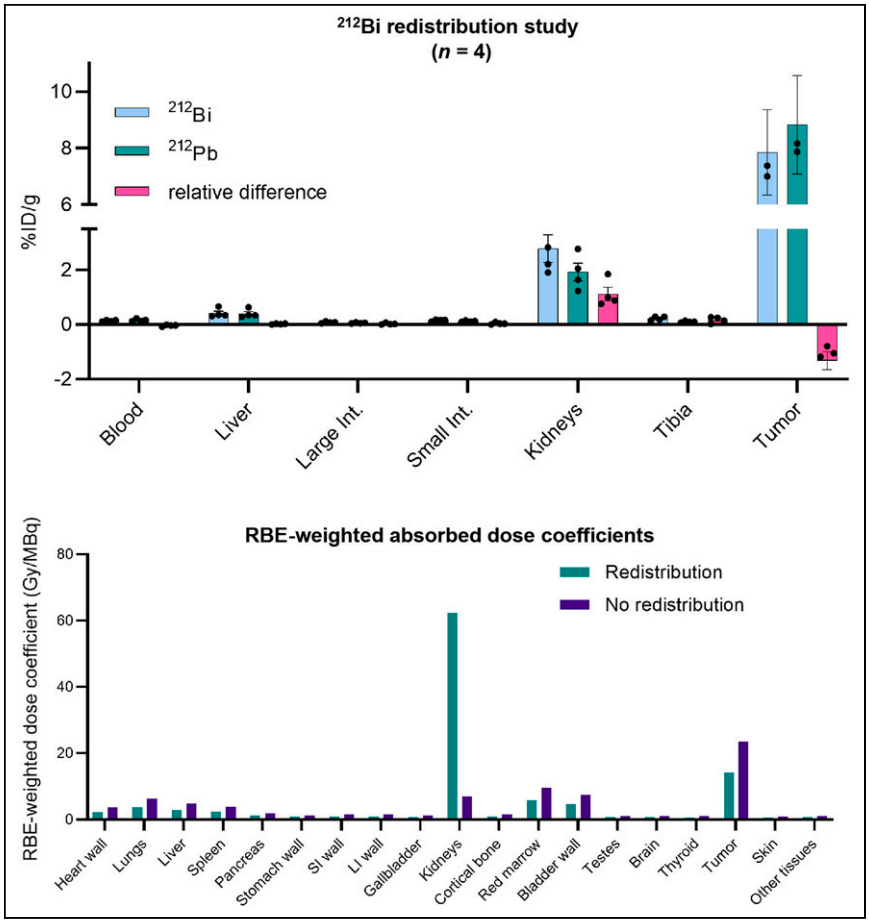

FIGURE 4. ^{212}Bi release and dosimetry estimations. (Top) Biodistribution data of ^{212}Bi, measured 15 min after death, and of ^{212}Pb. (Bottom) Estimated relative biological effectiveness–weighted absorbed dose coefficients for [^{212}Pb]Pb-DO3A-PEG7-Tz (in Gy-equivalent per MBq administered) estimated for different assumptions regarding redistribution of ^{212}Pb's progeny.

Therapy Study with [^{212}Pb]Pb-DO3A-PEG_7-Tz

A therapy study was conducted with [^{212}Pb]Pb-DO3A-PEG_7-Tz (single administration) comprising 5 arms (n = 8 per cohort) with 2 control and 3 therapeutic groups. The 2 control arms consisted of one group that received only 5B1-TCO and one that received an unspecific IgG-TCO mAb followed by administration of 1.1 MBq of [^{212}Pb]Pb-DO3A-PEG_7-Tz 3 d later. For PRT, the pretargeted mice received 1.1, 2.2, or 3.7 MBq of [^{212}Pb]Pb-DO3A-PEG_7-Tz. For these activities, the estimated relative biological effectiveness–weighted dose to the tumor tissue would be expected to induce a response (~20–100 Gy-equivalent) without producing excessive toxicity (Supplemental Fig. 8). The 4 groups that received a radioactive payload (3 d after mAb administration) were imaged 1 d after injection via Cerenkov luminescence imaging (Fig. 5A). The 4 therapeutic arms revealed that the Cerenkov luminescence imaging signal increased between the 3 dose levels. The IgG control arm showed unspecific accumulation in the liver, spleen, and kidneys.

The therapy study was accompanied by complementary imaging via PET using [^{64}Cu]Cu-DO3A-PEG_7-Tz (Fig. 5A) instead of relying on SPECT imaging with [^{203}Pb]Pb-DO3A-PEG_7-Tz. This was a practical consideration since PET imaging allows for easily quantifiable images, higher output, and shorter imaging times. We confirmed that the radiolabeling (Supplemental Fig. 2C)

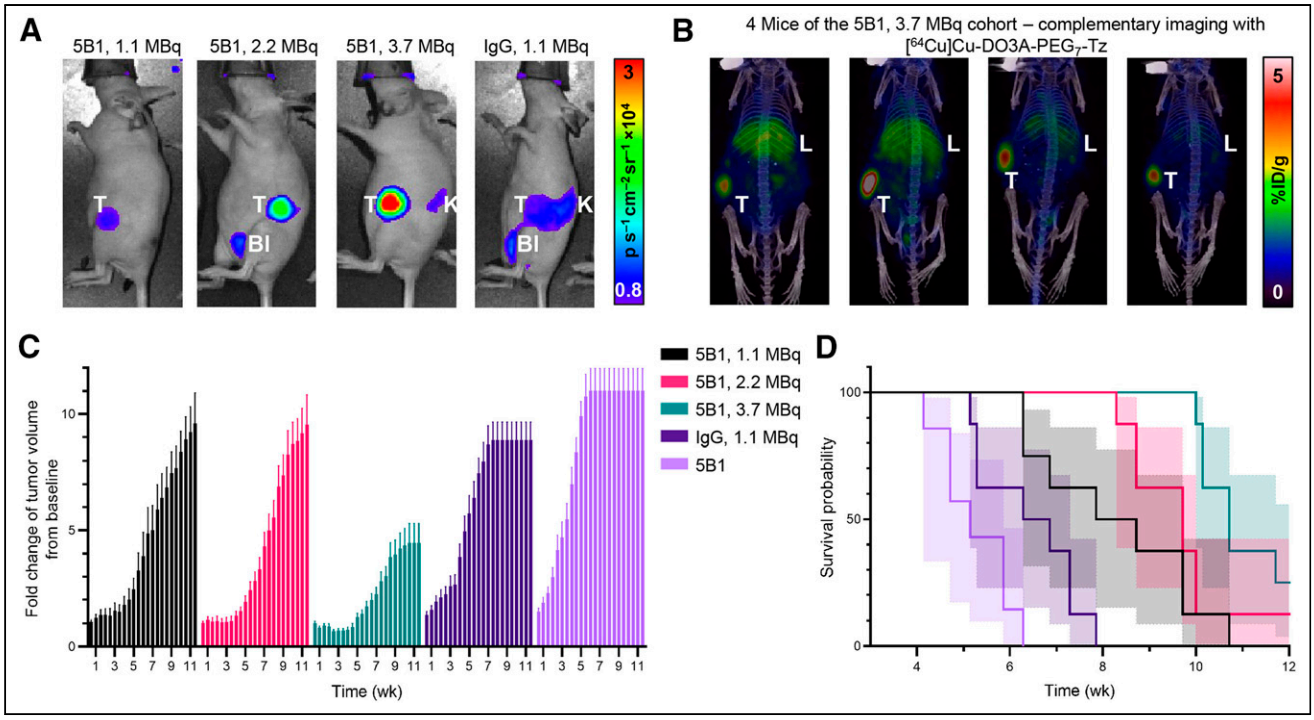

FIGURE 5. Therapy study: pretargeting with [^{212}Pb]Pb-DO3A-PEG$_7$-Tz. (A) Cerenkov luminescence imaging of 4 arms that received [^{212}Pb]Pb-DO3A-PEG$_7$-Tz (2 nmol) via pretargeting 24 h after injection. (B) Maximum-intensity projections (24 h after injection) of 4 mice (3.7-MBq cohort) injected with [^{64}Cu]Cu-DO3A-PEG$_7$-Tz 1 d after therapy to demonstrate complementary PET imaging. (C) Waterfall plot of fold change of tumor volume for each cohort. (D) Survival probability as function of time after Tz injection (n = 8 per cohort). Bl = bladder uptake; K = kidney uptake; T = tumor uptake.

and pharmacokinetics (Supplemental Fig. 9) are similar between the ^{64}Cu- and ^{203}Pb-labeled precursors. Consequently, dosimetry estimates and therapy monitoring can be pursued via either SPECT or PET imaging using ^{203}Pb or ^{64}Cu, respectively, greatly expanding the toolbox. Here, the mice were injected with the PET agent 1 d after receiving the therapeutic dose (4 d after 5B1-TCO administration) to circumvent interference with the Cerenkov luminescence imaging.

Three criteria were established requiring euthanasia of the mice: a tumor burden of more than 2,000 mm^3, weight loss of more than 20%, or a severe health condition (e.g., lethargy, petechiae, or infections). In the first week, the white blood cell count decreased for the 4 cohorts that received activity. The 3.7-MBq cohort was most affected, revealing a count of roughly 0.2×10^3 white blood cells per microliter. The population of platelets and red blood cells decreased minimally within the first 2 wk. By the third week, all cohorts had recovered from the initial impairment, as indicated by the normalized blood panel (Supplemental Fig. 10).

Compared with the 5B1-TCO control group, the PRT cohorts revealed a particular duration of tumor growth retardation, and the effect depended on the received activity. The delayed onset for tumor progression was roughly 5 wk for the 3.7-MBq cohort, 3.5 wk for the 2.2-MBq cohort, and 2.5 wk for the 1.1-MBq cohort (Fig. 5B; Supplemental Fig. 11). A growth suppression of almost 2 wk was observed for the IgG (+1.1 MBq of ^{212}Pb) control cohort; this finding can be attributed to the enhanced permeability and retention effect and stimulated immune response, as previously reported (*34*). After the onset of tumor progression, each cohort reached the endpoint in approximately 5 wk. On average, the median survival was 5.1 wk for the 5B1-TCO cohort and 6.5 wk for the IgG-TCO control cohort. The 1.1-, 2.2-, and 3.7-MBq [^{212}Pb]Pb-DO3A-PEG$_7$-Tz cohorts showed a median survival of 8.3, 9.7, and 10.7 wk, respectively. These data include mice euthanized before reaching the maximum tumor volume. Three mice of the 1.1-MBq cohort, 2 of the 2.2-MBq cohort, and 2 of the 3.7-MBq cohort developed ulcerating tumors. One mouse of the 3.7-MBq cohort and 2 of the IgG-TCO 1.1-MBq cohort showed lethargic behavior. One mouse of the 2.2-MBq cohort died on day 58 due to unidentified causes.

To investigate possible adverse effects of PRT, randomly selected mice from each cohort—after they reached their endpoint—were submitted alive for a comprehensive assessment by board-certified veterinary pathologists. This included a gross examination, a histopathologic examination of selected tissues of interest, and blood work (hematology and serum chemistry) analysis. The only significant changes that could be attributed to the treatment (i.e., radiation injury) in these mice were seen in the kidneys and ovaries (Fig. 6). The other macroscopic, microscopic, hematology, and serum chemistry changes observed in the evaluated mice were not considered treatment-related.

All the microscopically examined treated mice (n = 8) exhibited a bilateral minimal-to-mild tubulonephropathy with tubular epithelial degeneration and necrosis (cellular sloughing, cytoplasmic swelling, pallor, condensation or hypereosinophilia, karyorrhexis, karyolysis or karyomegaly, or attenuation). These changes affected a minimal to mild portion (≈1%–≤10%) of the renal tubules—mainly those found at the corticomedullary junction. These lesions were not observed in the microscopically examined 5B1-TCO control mice (n = 3). These findings resemble renal injuries previously associated with α-emitter treatments in mice, including mice administered ^{212}Pb and ^{225}Ac (*35,36*). Although some mice were slightly more affected than others, the treatment

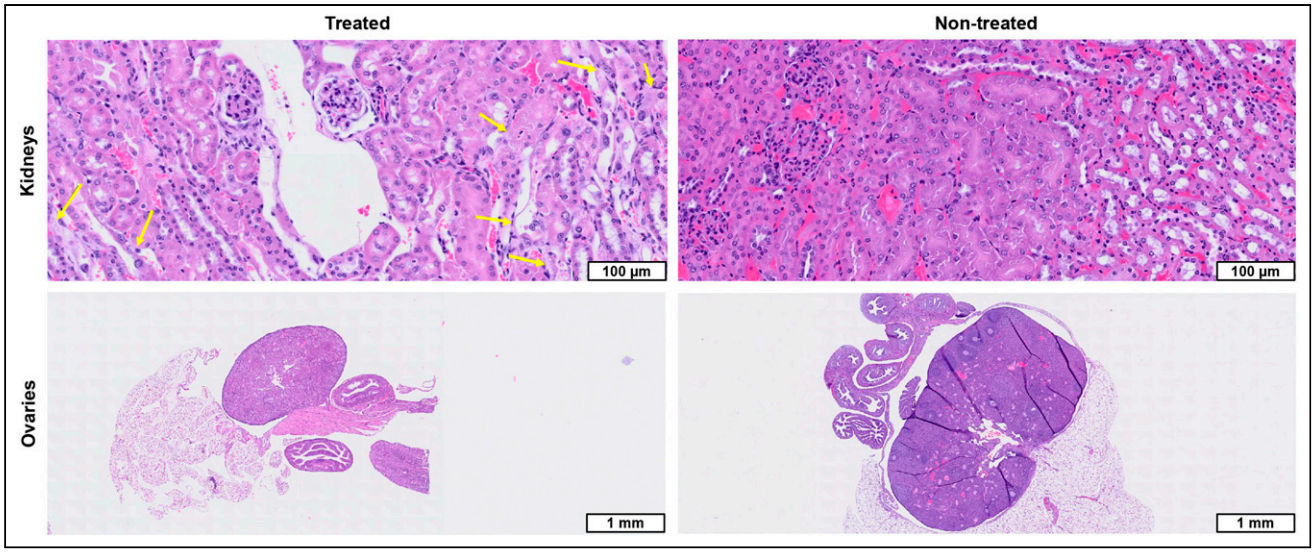

FIGURE 6. Representative histology results. Representative histology of hematoxylin- and eosin-stained kidney (top) and ovarian (bottom) sections of BxPC-3 tumor–bearing female athymic nude mice. (Left) Mice treated with ^{212}Pb. (Right) Control group. Histopathology of kidneys revealed multifocal, minimal-to-mild tubular injury (arrows) affecting approximately 1%–10% of tubules. Control animals showed histologically normal kidneys. Histopathology of treated ovaries revealed diffuse marked ovarian atrophy with complete loss of follicles and corpora lutea.

dosage did not seem to have significantly affected the severity of the kidney lesions. These lesions also did not seem to substantially affect the renal function of these animals, as there were no apparent signs of renal toxicity in the serum chemistry results.

All microscopically examined ovaries from the treated mice (n = 9) exhibited marked atrophy. These ovarian changes were not observed in the microscopically examined 5B1-TCO control mice (n = 6). Ovarian atrophy can be caused by radiation because of nonreversible injury to germ cells (*37*). Ovaries are radiosensitive organs, and their atrophy has been described as an effect of some radioimmunotherapies in mice (*38*). As all examined ovaries were markedly affected, the treatment dose did not seem to have substantially affected the severity of the ovarian lesions.

The pathology report further highlights that fractionated dosing of [^{212}Pb]Pb-DO3A-PEG$_7$-Tz at 1- to 2-wk intervals could decrease toxicity while possibly increasing the therapeutic response. Reimaging of selected mice 10 wk after receiving the therapeutic dose confirmed that their tumors still highly express the carbohydrate cell surface antigen 19-9 (Supplemental Fig. 12), indicating the feasibility of fractionated dosing.

CONCLUSION

The elementary match pair ^{212}Pb and ^{203}Pb has demonstrated great potential to advance theranostics and promote the translation of TAT. For the relatively short-lived therapeutic nuclide ^{212}Pb, PRT appears to be a promising strategy because of its rapid delivery of the radioactive payload and minimal off-targeting.

Here, we used a xenografted PDAC mouse model and the TCO-modified mAb 5B1 to enable pretargeting with the Tz-based radiotracer [^{203}Pb]Pb-DO3A-PEG$_7$-Tz.

In a single administration study, the efficiency and safety of PRT with ^{212}Pb were evaluated. With the highest administered dose of 3.7 MBq, the average survival time could be doubled compared with the control cohort while maintaining radiotoxicity within acceptable limits. Furthermore, we demonstrated that even when using a noninternalizing vector, the limited redistribution of the daughter nuclide ^{212}Bi does not lead to marked reduction in antitumor potency and does not lead to marked increases in normal-organ toxicity.

The short half-life of ^{212}Pb (10.6 h) would allow for a controlled dose fractionation and weekly-to-biweekly injections. On this regimen, side effects can be minimized, therapy progress can be monitored exactly, and the tumor burden can be further reduced until eventually eliminated. Recently, Keinänen et al. reported on a pretargeting strategy harnessing $^{64/67}$Cu in a colorectal cancer mouse model. They revealed that fractionated dosing with the therapeutic nuclide resulted in prolonged tumor suppression (*9*). Studies with ^{212}Pb administration in biweekly cycles (fractionated dosing) are under way.

This foundational study demonstrated the feasibility and safety of pretargeted TAT with ^{212}Pb in PDAC while considering dose limitations and potential adverse effects.

DISCLOSURE

This work was supported by the donation of Diane and James Rowen (David Bauer and Jason Lewis), the Tow Foundation Fellowship Program (David Bauer), and NCI R35 CA232130 (Jason Lewis). The MSK Small-Animal Imaging Core Facility's technical services were partly funded through NIH Cancer Center support grant P30 CA008748 and NIH Shared Instrumentation grants S10 RR02892-01 and S10 OD016207-01. Technical services provided by the MSK Analytic NMR Core Facility were funded in part through NIH/NCI Cancer Center support grant P30 CA008748. Jason Lewis holds intellectual property related to the application of click and radiopharmaceutical chemistry (patent US11135320B2). This work was supported by Perspective Therapeutics Inc. (Mengshi Li and Michael Schultz are employees). No other potential conflict of interest relevant to this article was reported.

ACKNOWLEDGMENTS

We thank the U.S. Department of Energy Isotope Program (Isotope R&D Production) and Perspective Therapeutics, Inc. for providing the ^{224}Ra/^{212}Pb lead generators as well as Suzanne E. Lapi and Shefali Saini (both at the University of Alabama at Birmingham, Department of Radiology) and John S. Wilson (University of Alberta, Department of Oncology) for providing ^{203}Pb. Furthermore, we thank George Sukenick and Rong Wang (MSK Analytical NMR Core Facility) for supporting NMR and mass spectrometry; the Laboratory of Comparative Pathology (MSK Core Facility) for evaluating the therapy data; and Kishore Pillarsetty, Edwin C. Pratt, Garon Scott (MSK Radiology), and Lawson Spare (ANSTO) for providing advice and support.

KEY POINTS

QUESTION: Is pretargeting a feasible strategy for the theranostic matched pair $^{203/212}$Pb to enable combined imaging and therapy in an adenocarcinoma mouse model?

PERTINENT FINDINGS: Pretargeting is a suitable delivery approach for the short-lived radionuclide ^{212}Pb. This foundational study demonstrates the feasibility and safety of pretargeting TAT with ^{212}Pb—accompanied by complementary imaging with ^{203}Pb (and ^{64}Cu)—in PDAC while considering dose limitations and potential adverse effects.

IMPLICATIONS FOR PATIENT CARE: Pretargeting with radiolead is a promising strategy to improve patient care, especially for cancer entities with currently limited treatment options, such as PDAC. Upcoming studies will elucidate the benefit of dose fractionation, which will minimize side effects while the tumor burden is further reduced until eventually eliminated.

REFERENCES

1. Ganesh K, Massague J. Targeting metastatic cancer. *Nat Med.* 2021;27:34–44.
2. Juzeniene A, Stenberg VY, Bruland OS, Larsen RH. Preclinical and clinical status of PSMA-targeted alpha therapy for metastatic castration-resistant prostate cancer. *Cancers (Basel).* 2021;13:779.
3. Raja C, Graham P, Abbas Rizvi SM, et al. Interim analysis of toxicity and response in phase 1 trial of systemic targeted alpha therapy for metastatic melanoma. *Cancer Biol Ther.* 2007;6:846–852.
4. Jurcic JG, Rosenblat TL. Targeted alpha-particle immunotherapy for acute myeloid leukemia. *Am Soc Clin Oncol Educ Book.* 2014:e126–e131.
5. Kim YS, Brechbiel MW. An overview of targeted alpha therapy. *Tumour Biol.* 2012;33:573–590.
6. McNeil BL, Robertson AKH, Fu W, et al. Production, purification, and radiolabeling of the ^{203}Pb/^{212}Pb theranostic pair. *EJNMMI Radiopharm Chem.* 2021;6:6.
7. Kokov KV, Egorova BV, German MN, et al. ^{212}Pb: production approaches and targeted therapy applications. *Pharmaceutics.* 2022;14:189.
8. Poty S, Carter LM, Mandleywala K, et al. Leveraging bioorthogonal click chemistry to improve ^{225}Ac-radioimmunotherapy of pancreatic ductal adenocarcinoma. *Clin Cancer Res.* 2019;25:868–880.
9. Keinänen O, Fung K, Brennan JM, et al. Harnessing ^{64}Cu/^{67}Cu for a theranostic approach to pretargeted radioimmunotherapy. *Proc Natl Acad Sci USA.* 2020;117:28316–28327.
10. Sarrett SM, Keinanen O, Dayts EJ, et al. Inverse electron demand Diels-Alder click chemistry for pretargeted PET imaging and radioimmunotherapy. *Nat Protoc.* 2021;16:3348–3381.
11. Houghton JL, Zeglis BM, Abdel-Atti D, Sawada R, Scholz WW, Lewis JS. Pretargeted immuno-PET of pancreatic cancer: overcoming circulating antigen and internalized antibody to reduce radiation doses. *J Nucl Med.* 2016;57:453–459.
12. Sarantis P, Koustas E, Papadimitropoulou A, Papavassiliou AG, Karamouzis MV. Pancreatic ductal adenocarcinoma: treatment hurdles, tumor microenvironment and immunotherapy. *World J Gastrointest Oncol.* 2020;12:173–181.
13. Faustino-Rocha A, Oliveira PA, Pinho-Oliveira J, et al. Estimation of rat mammary tumor volume using caliper and ultrasonography measurements. *Lab Anim (NY).* 2013;42:217–224.
14. Larson SM, Carrasquillo JA, Cheung NK, Press OW. Radioimmunotherapy of human tumours. *Nat Rev Cancer.* 2015;15:347–360.
15. Emami B, Lyman J, Brown A, et al. Tolerance of normal tissue to therapeutic irradiation. *Int J Radiat Oncol Biol Phys.* 1991;21:109–122.
16. Yoo J, Reichert DE, Welch MJ. Comparative in vivo behavior studies of cyclen-based copper-64 complexes: regioselective synthesis, x-ray structure, radiochemistry, log P, and biodistribution. *J Med Chem.* 2004;47:6625–6637.
17. Jones-Wilson TM, Deal KA, Anderson CJ, et al. The in vivo behavior of copper-64-labeled azamacrocyclic complexes. *Nucl Med Biol.* 1998;25:523–530.
18. Koźmiński P, Gaweda W, Rzewuska M, et al. Physicochemical and biological study of ^{99m}Tc and ^{68}Ga radiolabelled ciprofloxacin and evaluation of [^{99m}Tc]Tc-CIP as potential diagnostic radiopharmaceutical for diabetic foot syndrome imaging. *Tomography.* 2021;7:829–842.
19. Nikolaychuk PA. The revised potential-pH diagram for Pb-H_2O system. *Ovidius University Annals of Chemistry.* 2018;29:55–67.
20. Lipowska M, Klenc J, Marzilli LG, Taylor AT. Preclinical evaluation of ^{99m}Tc(CO)$_3$-aspartic-*N*-monoacetic acid, a renal radiotracer with pharmacokinetic properties comparable to ^{131}I-*o*-iodohippurate. *J Nucl Med.* 2012;53:1277–1283.
21. Imberti C, Chen YL, Foley CA, et al. Tuning the properties of tris(hydroxypyridinone) ligands: efficient ^{68}Ga chelators for PET imaging. *Dalton Trans.* 2019;48:4299–4313.
22. Membreno R, Cook BE, Zeglis BM. Pretargeted radioimmunotherapy based on the inverse electron demand Diels-Alder reaction. *J Vis Exp.* 2019;143:10.3791/59041.
23. Szucs Z, van Rooyen J, Zeevaart JR. Recoil effect on beta-decaying in vivo generators, interpreted for ^{103}Pd/^{103m}Rh. *Appl Radiat Isot.* 2009;67:1401–1404.
24. Bartoś B, Lyczko K, Kasperek A, Krajewski S, Bilewicz A. Search of ligands suitable for ^{212}Pb/^{212}Bi in vivo generators. *J Radioanal Nucl Chem.* 2013;295:205–209.
25. Auranen K, McCutchan EA. Nuclear data sheets for A=212. *Nucl Data Sheets (NY NY).* 2020;168:117–267.
26. Schwartz J, Jaggi JS, O'Donoghue JA, et al. Renal uptake of bismuth-213 and its contribution to kidney radiation dose following administration of actinium-225-labeled antibody. *Phys Med Biol.* 2011;56:721–733.
27. Su FM, Beaumier P, Axworthy D, Atcher R, Fritzberg A. Pretargeted radioimmunotherapy in tumored mice using an in vivo ^{212}Pb/^{212}Bi generator. *Nucl Med Biol.* 2005;32:741–747.
28. Ruble G, Wu C, Squire RA, Ganswo OA, Strand M. The use of ^{212}Pb-labeled monoclonal antibody in the treatment of murine erythroleukemia. *Int J Radiat Oncol Biol Phys.* 1996;34:609–616.
29. Mirzadeh S, Kumar K, Gansow OA. The chemical fate of ^{212}Bi-DOTA formed by β-decay of ^{212}Pb(DOTA)$^{2-}$. *Radiochim Acta.* 1993;60:1–10.
30. Keenan MA, Stabin MG, Segars WP, Fernald MJ. RADAR realistic animal model series for dose assessment. *J Nucl Med.* 2010;51:471–476.
31. Carter LM, Crawford TM, Sato T, et al. PARaDIM: a PHITS-based Monte Carlo tool for internal dosimetry with tetrahedral mesh computational phantoms. *J Nucl Med.* 2019;60:1802–1811.
32. Bartlett RM, Bolch WE, Brill AB, et al. *MIRD Primer 2022: A Complete Guide to Radiopharmaceutical Dosimetry.* Society of Nuclear Medicine and Molecular Imaging; 2022.
33. Cloutier RJ, Smith SA, Watson EE, Snyder WS, Warner GG. Dose to the fetus from radionuclides in the bladder. *Health Phys.* 1973;25:147–161.
34. Heneweer C, Holland JP, Divilov V, Carlin S, Lewis JS. Magnitude of enhanced permeability and retention effect in tumors with different phenotypes: ^{89}Zr-albumin as a model system. *J Nucl Med.* 2011;52:625–633.
35. Milenic DE, Molinolo AA, Solivella MS, et al. Toxicological studies of ^{212}Pb intravenously or intraperitoneally injected into mice for a phase 1 trial. *Pharmaceuticals (Basel).* 2015;8:416–434.
36. Cheal SM, McDevitt MR, Santich BH, et al. Alpha radioimmunotherapy using ^{225}Ac-proteus-DOTA for solid tumors: safety at curative doses. *Theranostics.* 2020;10:11359–11375.
37. Dixon D, Alison R, Bach U, et al. Nonproliferative and proliferative lesions of the rat and mouse female reproductive system. *J Toxicol Pathol.* 2014;27(suppl):1S–107S.
38. Santich BH, Cheal SM, Ahmed M, et al. A self-assembling and disassembling (SADA) bispecific antibody (BsAb) platform for curative two-step pretargeted radioimmunotherapy. *Clin Cancer Res.* 2021;27:532–541.